Method for Crater Detection From Martian Digital Topography Data Using Gradient Value/Orientation, Morphometry, Vote Analysis, Slip Tuning, and Calibration

Goran Salamunićcar, *Member, IEEE*, and Sven Lončarić, *Senior Member, IEEE*

***Abstract*—Recently, all the craters from the major currently available manually assembled catalogs have been merged into the catalog with 57 633 known Martian impact craters. This paper presents a new crater detection algorithm (CDA) for the search of still uncataloged impact craters. The CDA is based on fuzzy edge detectors and Radon/Hough transform and utilizes digital topography data instead of image data. The critical parts of the method providing increased accuracy are as follows: 1) gradient-value/orientation-based techniques; 2) automated morphometry measurements of depth/diameter ratio, circularity, topographic cross-profile, rim, central peak, and radial range where the crater is preserved; 3) circularity analysis of votes in parameter space; 4) slip tuning of detected craters' parameters; and 5) calibration which partially compensates differences in morphology between small and large craters. Using the framework for the evaluation of CDAs, in comparison with prior work, the proposed detector shows the following: 1) significantly larger area under the free-response receiver operating characteristics (AUROC) and 2) significantly larger number of correct detections. Using the Mars Orbiter Laser Altimeter data as input, the CDA proposed numerous candidates for GT-57633 catalog extension. After the manual survey of all proposed craters and rejection of false detections, 57 592 impact craters were confirmed as correct detections. The accompanying result to the CDA is a new GT-115225 catalog.**

***Index Terms*—Crater detection algorithms (CDAs), image edge analysis, Mars, object detection, Radon/Hough (RH) transform.**

I. Introduction

With each new lunar and planetary mission, the volume of images, topography, and other acquired data significantly increases. Image analysis plays an important role in methods for archiving, retrieval, processing, and interpretation of large amounts of image data. Examples of such remote sensing data include satellite imagery acquired in the visible spectrum, infrared spectrum, digital elevation map (DEM) data, and radar sounder data. One of the most important problems in image analysis in lunar and planetary applications is the classification of satellite images [1], wherein various learning methods are an important subject of recent research [2]. This paper addresses the problem of crater detection from the Mars Orbiter Laser Altimeter (MOLA) DEM data. Other research works on the same kind of data (MOLA) for studying Martian surface structures including impact craters are presented in [3] and [4]. A similar problem of ellipse detection in the identification of oceanic eddies is presented in [5].

A. Previous Research on CDAs

In lunar and planetary science, some of the most studied features are impact craters. This makes crater detection algorithms (CDAs) an important subject of recent scientific interest, as evident from the numerous recent publications in the field. An overview of a large body of CDA-related literature has recently been assembled, including a tabular overview of 73 CDA publications from numerous authors, as given in [6], and 12 additional CDA publications, as given in [7]. In the meantime, the collection has been expanded by the following: feature detection using sun shading [8], 3-D crater database [9], [10], search for potential Norwegian craters [11], crater detection by a boosting approach [12], [13], automatic survey of craters on Mars [14], [15], automatic detection of subkilometer craters on Mars from high-resolution visual images [16], automated system for cataloging impact craters using the DEM of Mars [17], as well as the reports on our ongoing work [18]–[21]. CDA applications range from dating planetary surfaces [22]–[24] and searching for still unknown impact craters on Earth [25] to autonomous landing on planets [26], [27] and asteroids [28], localization of rovers using descent and surface-based image data [29], autonomous rover navigation [30], registration between different coordinate systems [31], and advanced statistical analyses [32], [33].

Our previous research on CDA includes the work on image-processing algorithms [34], wherein directional first derivation of surface outlined the possibility to be used in the work on the CDA. Our first CDA [35] was based on Frei–Chen [36] gradient edge detector and Radon/Hough (RH) transform [37]. It was used within the framework for the evaluation of CDAs [6]. In order to compare overall performance, five new CDAs were implemented [38] based on the following gradient edge detectors [39]: 1) pixel difference; 2) separated pixel difference;

Manuscript received July 9, 2009; revised October 7, 2009 and November 11, 2009. First published February 2, 2010; current version published April 21, 2010.

G. Salamunićcar is with AVL-AST d.o.o., 10020 Zagreb-Novi Zagreb, Croatia, with the University of Zagreb, 10000 Zagreb, Croatia, and also with the Polytechnic of Zagreb, 10000 Zagreb, Croatia (e-mail: gsc@ieee.org).

S. Lončarić is with the Department of Electronic Systems and Information Processing, Faculty of Electrical Engineering and Computing, University of Zagreb, 10000 Zagreb, Croatia (e-mail: sven.loncaric@fer.hr).

Color versions of one or more of the figures in this paper are available online at http://ieeexplore.ieee.org.

Digital Object Identifier 10.1109/TGRS.2009.2037750

3) Roberts; 4) Prewitt; and 5) Sobel. These CDAs were used for the development and testing of the following methods: 1) circular-consistency (circularity) measurements and slip tuning [18]; 2) gradient value and orientation measurements [20]; and 3) morphometry (which includes circularity) and vote-analysis measurements and calibration [21]. Furthermore, five new CDAs were implemented based on the following gradient edge detectors [39]: 1) Abdou; 2) Argyle; 3) Macleod; 4) derivative of Gaussian (DroG); and 5) Canny. Additionally, we implemented five new CDAs based on the following compass edge detectors [39]: 1) Kirsch; 2) Prewitt; 3) Robinson 3-Level (based on gradient Prewitt); 4) Robinson 5-Level (based on gradient Sobel); and 5) Nevatia–Babu. We also implemented the version of CDA based on Canny [40] which uses a compass edge detector instead of gradient edge detector and a CDA based on the Shen–Castan [41] edge detector. It should be noted that all the edge detectors we used have been developed for image analysis. In this paper, they are used for elevation data.

B. Previous Research on Crater Catalogs

The most closely related to this paper are CDAs from [31] and [14], wherein the input is also MOLA data; only these two cases actually demonstrated the capability to process data globally. With CDA from [14], a global catalog with 75 919 craters has additionally been produced. The difference between [14] and the work presented in this paper is that our starting point was the GT-57633 catalog [7]. In this way, the newly obtained catalog will be much more complete. Each crater from the GT-57633 catalog is manually confirmed, and the catalog already contains all the craters from catalogs by Barlow (B), Rodionova (R), Boyce (C), Kuzmin (K), and our previous work (N)[7]. Another difference is the manual survey of each crater proposed by the CDA from this paper, before rejection or acceptance as correct detection. Related work regarding the search for still uncataloged Martian craters is also contained in [42]. However, no CDA is in use in that case. It is also to be expected that CDAs that utilize visual images, as, for example, [43], could be used in the future for assembling global catalogs.

C. Crater Detection From Topography Data

The CDA proposed in this paper uses the global Martian DEM. The main disadvantages of this data set are as follows: 1) The highest available resolution for this data set is 1/128° (∼500 m/pixel at the equator) whereas there are already available image mosaics with a resolution of 1/256° (∼250 m/pixel at the equator) globally and a much higher resolution (satellite images up to ∼30 cm/pixel) for specific regions; 2) the DEM is interpolated, and a large proportion of cells have elevation values that are not based on a direct laser measurement; and 3) the laser measurement coverage is not uniform, which results in the existence of numerous areas where the topography does not reflect reality—they look like smudges, as can be seen in Fig. 7 (image (2) MOLA segment). A direct consequence of these disadvantages of the chosen data set is that numerous (particularly small) craters will not be detectable by DEM-based CDAs.

On the other hand, there are also numerous quasi-circular depressions (QCDs), found using MOLA data [44], that have no obvious structural representation in visible images of Mars. These QCDs were interpreted as being most probably buried impact craters. An additional argument for this hypothesis comes from the MARSIS radar sounder evidence of buried basins in the northern lowlands of Mars [45], which corresponds to some previously found QCDs. In our previous work [7], for the crater S042146C01833Y2007S, which was discovered by Frey *et al.* [44] as a QCD that is not visible on the Mars Digital Image Model (MDIM) image, we found that the THEMIS-DIR image clearly shows a crater rim as evidence that this, indeed, is an impact crater. All these findings influenced our decision to choose MOLA data rather than much better quality image mosaics.

Another factor was the recent work on extracting DEMs from high-resolution satellite stereo images [46] and similar results of some recent missions such as Mars Express. It is also to be expected that DEMs will soon be available, with similar or even higher resolution, from missions to other lunar and planetary bodies, owing to instruments such as the Mercury Laser Altimeter and the Lunar Orbiter Laser Altimeter.

An additional important point is that the work on detecting craters from DEMs is, in principle, much easier than detecting them from imagery data, because craters are landforms that can be defined in terms of terrain morphometric attributes calculated from the DEM [47]. Such an approach avoids numerous problems inherent to the detection of craters from visual images, such as illumination. The consequence of such problems is that the detection of craters from visual images globally for the whole planet is still an unsolved problem. Based on the aforementioned arguments, we based the proposed CDA on DEM data.

D. Main Motivation for Our Work

The main motivation for the work presented in this paper can be outlined as a summary of the three previous paragraphs: 1) There is still no robust CDA available (several research groups work in this young field); therefore, the necessity for novel methods or improvements of previous ones is justified; 2) a complete global catalog of Martian craters is of particular importance to lunar and planetary science community (several teams aim to achieve this); therefore, the work on CDA in order to be used as an assisting tool for this purpose is justified; and 3) numerous craters which are not visible on visual images can be detected using DEM; therefore, this is a justification and reason for choosing DEM data. The strategy is to find large and middle-sized still undiscovered craters first, which can be detected using lower resolution DEM-based CDA and then to proceed to higher resolution visual images and smaller craters.

E. Exposition of the Problem

On Mars, there are lots of different crater shapes according to their ejecta structures (pedestal, pancake, rampart, lobate, fluidized, radial or lunarlike, transitional, or diverse) and interior morphologies (central peaks, peak rings, central pits, and wall terraces) [48]. In addition, there is a simple–complex

transition from the smallest mostly very circular bowl-shaped craters toward the largest multiring impact craters [49]. All this diversity increases even more because each crater can be in any of many degradation states, from the recent craters with well-preserved morphometry characteristics to the degraded ones, partially or completely erased by newer craters or other geological processes. The proposed CDA processes a global DEM, therefore necessitating robustness in order to cover at least the most common patterns in craters' shapes.

An additional issue is computational efficiency. In order to perform a systematic search for all possible Longitude–Latitude–Radius (LLR) combinations using 1/128° MOLA data (23 040 × 46 080 pixels) and radius range between 2 and 28 pixels (the largest we used), as well as downsampled MOLA data between 1/64° and 4° with radius range between 14 and 28 pixels (the rest is covered by previous DEMs), there are altogether 33 973 842 150 combinations to check. For each of these combinations, the proposed CDA must process the appropriate section of DEM in order to decide if it is an impact crater or not, and if it is, the CDA estimates the probability that the detected feature indeed is an impact crater. All this makes an important requirement for almost real-time performance for individual LLR combinations.

F. Main Achievements of Our Work

The main achievements of this paper are the following: 1) the proposed DEM-based CDA with high detection rate; 2) a very efficient implementation of the proposed CDA (the achieved performance on a 4-CPU 8-GB personal computer (PC) is that the computations for 1/128° MOLA data are done in less than 9 h, wherein each LLR combination, on average, is processed in less than 1 μs); and 3) the resulting GT-115225 catalog of Mars crater data. Numerous previously uncataloged impact craters were successfully detected, and the previous GT-57633 catalog was significantly extended with 57 592 new entries. In order to achieve this, in comparison with existing methods, it was necessary to do the following: 1) improve the detection of much degraded craters and incomplete craters wherein large segment(s) of a crater were completely missing and 2) achieve better detection of very small craters that can still be detected using DEM data.

The rest of this paper is organized as follows. In Section II, the methods developed and then used during the work on the CDAs are presented in detail. The results are presented in Section III, and the conclusion is given in Section IV.

II. METHODS

The overall architecture of the new CDA is shown in Fig. 1 and described in the next section, followed by the presentations of new methods for fuzzy edge detection and RH transform, morphometry and parameter-space analysis, calibration, and slip tuning.

A. Proposed Method

In module 1 shown in Fig. 1, the edge detection is performed. The result is the representation wherein the 3-D shape of an impact crater is transformed into a 2-D circle. In module 2 shown in Fig. 1, for each given radius (from a preselected range) using RH transform, each circle of such or very similar radius is transformed into the parameter space. Therein, the locations of local maxima correspond to the locations of crater centers. Having the location and radius, this module searches for local maxima in order to find initial crater candidates. The main purpose of these two modules is to significantly reduce the number of LLR combinations that will be processed in the following modules. The main problem is if an LLR combination that corresponds to correct detection is not passed through to the following modules. In order to address this problem, we implemented the following: 1) a large number of edge detectors in order to choose the best detector and 2) fuzzy versions of these edge detectors and RH transform which additionally utilize the value and the orientation of a gradient. This significantly reduces the influence of other nearby craters and other geological features with steep slopes during the detection of a particular crater and almost completely solves the aforementioned problem.

Module 3 shown in Fig. 1 receives initial crater candidates and, owing to the significantly smaller number of LLR combinations at this stage, can perform computationally more

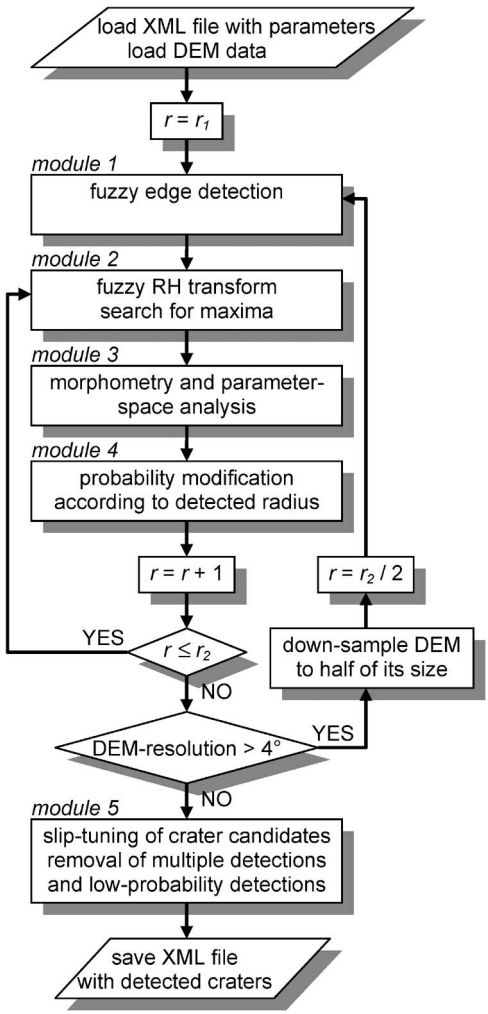

Fig. 1. Schematic flow diagram of overall organization and processing steps for our DEM-based CDA.

demanding pattern recognition. The main task of this module is to provide a clear distinction between true and false detections. It is similar to the recent work on one-class classification for mapping a specific land-cover class [50], because we detect only one class (craters) and we are not interested in modeling other classes (noncraters). Another distinction according to the most common usage of support vector machines and other machine-learning methodologies is that this module also provides an estimation of the probability that each detected feature indeed is an impact crater. At this stage, we use a modular boostinglike approach, where an arbitrary number of individual detectors of crater specific features (such as crater rim, central peak, etc.) can be easily combined. Individual detectors are used to estimate the probability of specific crater properties, using DEM or parameter space. Finally, the estimation of the probability (that a detected feature is an impact crater) is (similarly to the Naive Bayes' approach) a product of individual probabilities. All these individual detectors are modeled using a number of conditionally free parameters, and optimal values for these parameters are found when the CDA is completed. The final result of module 3 is a probability estimate that the detected feature is a crater.

The purpose of module 4 shown in Fig. 1 is the modification of crater-candidate probability according to the crater radius. This module maps the original probability value to a new value, in order to obtain a desired target probability density function showing the probability of craters of certain diameters in the resulting catalog.

Module 5 shown in Fig. 1 performs the final tuning of crater candidates. The purpose of this step is to assign more precise coordinates, radii, and probability values to craters. During the development of our CDA, for evaluation purposes, we used the framework for the evaluation of CDAs [6]. Among others, this includes the GT-17582 catalog and graphical representation with up to 17 582 (τ) correct detections and up to $10 \cdot \tau$ false detections. This means that we were not able to use more than 193 402 $(11 \cdot \tau)$ craters for evaluation; hence, we decided that module 5 has to select only this number of craters with the highest probability and delete others. This is not a limitation, as from our experience with working on crater catalogs [6], [7], we know that the number of correct detections must be considerably smaller than this. The automatic search for duplicates and the removal of such cases, as well as the sorting of craters at the end, are also parts of module 5.

For large data sets, one approach can be to divide them into smaller segments which are processed individually. In order to avoid additional complexity for numerous modules and to make overall processing as fast as possible, we decided to upload everything into RAM. To achieve this, it is of particular importance for each pixel to be assigned as small amount of data as possible. The MOLA data are stored as 2 bytes/pixel. For storing the results of fuzzy edge detection, we are using a 1-byte/pixel (0 means that the edge is not detected): 1) 4 bits for the value of a gradient and 2) 4 bits for the orientation of a gradient at this point. For storing the results of fuzzy RH transform, we are using 1 byte/pixel again. In order to speed up computations, the following were performed: 1) we have developed our CDA as a 64-bit application; 2) all modules shown in Fig. 1 were developed as multithreaded algorithms and optimized so that, on a PC with four CPUs, the overall processing time is almost four times shorter than on a PC with one CPU; and 3) the edge detection is computed only once per DEM resolution.

The variables shown in Fig. 1 are as follows: 1) radius r; 2) minimal radius r_1; and 3) maximal radius r_2. The user defines r_1 and r_2, while at the run time, r is computed. In the first pass for initial DEM, the CDA searches for craters with $r = r_1$. In the next pass, the CDA searches for craters with r's that are one pixel larger. In the last pass for initial DEM, the CDA searches for craters with $r = r_2$. Once DEM is downsampled onto half of its size, craters that were r_2 pixels large become $r_2/2$ pixels large. Therefore, after the downsampling of DEM, r is initialized to this value and not to r_1, which can be significantly smaller. Another variable of interest for numerous modules is radial resolution rr. With $rr(2 \cdot r \cdot \pi)$, it is defined how many pixels there are on a circle with radius equal to r. This defines rr directions from the center of a crater to the location on the crater's rim, in which samples of elevation (or parameter space) are taken in the subsequent steps. In order to improve the capability of detection of small craters, the following are endured: 1) The samples are not taken directly from the data sets but estimation is performed using the values from the nearest pixels and the relative distance between an exactly computed location and the centers of these pixels, and 2) the range of rr is limited to be not smaller than the certain minimum value in order to oversample the craters with diameters smaller than some predefined size. In principle, for a smaller r_1, CDA is capable of detecting smaller craters, and for a larger r_2, its computations are more precise up to certain limits, but unfortunately also slower.

From http://rac.tvz.hr/index.php?pred=15138, the source code (Craters3_88.zip) can be downloaded, as well as catalogs GT-17582, GT-57633, and GT-115225. The complete implementation in C++ including all implementation details is out of the scope of this paper, while the most important parts will be elaborated in the following sections.

B. Module 1: Fuzzy Edge Detection

For the edge detectors from this paper, we found that the optimal values of a gradient for a threshold are between 20‰ and 40‰. The 1‰ is defined as 1 m of elevation change over 1 km of distance change. We also found that the gradients which are more than 10‰ (1%) larger than the gradients used for the threshold usually do not belong to craters but to other geological features. Therefore, the value of a gradient that we are storing for each pixel is limited to a value that is 1% larger than the optimal gradient which was used as a threshold. In order to store the values from this range using only 4 bits, as described in the previous section, this range is divided into 16 equal subranges, so that each value can be mapped to the appropriate subrange. Similarly, the orientation of a gradient is also stored for each pixel using only 4 bits. The complete range of 360° is divided into 16 equal subranges, so that each value can be mapped to the appropriate subrange. With this, the job of fuzzy edge detection is completed, and the processing of fuzzy RH transform can begin.

C. Module 2: Fuzzy RH Transform

In a classical RH implementation, during summation, each pixel from the edge is attributed with weight factor 1. Instead, in this method, the actual value of the gradient value [31] is used. In addition, gradient orientation [8] is also taken into account. During this summation, the idea is to take into account only those pixels which are parts of the detected edge which belongs to the crater we expect at this location. For each pixel on the edge, the method computes the difference between the gradient orientation and the direction of the crater center, rounded to discrete values indexed in the range of 0–15. This range is the same as the range for storing gradient orientation, in order to simplify computations. At this point, during the summation, there are numerous possibilities on how to combine these index differences and gradient values using different weight factors. The range of the weight factors, in principle, is not defined; thus, we try different values. The best results were obtained when, for index differences of 0, 1, 2, 3, …, 15, the selected weight factors were 3, 2, 1, 0, …, 0, respectively. At the end, the discrete gradient value in the range from 0 to 15 is multiplied with the computed weight factors which depend on the gradient orientation at this particular point of the crater rim. Finally, the value for a fuzzy RH array is equal to the sum of such contributions from gradient value and gradient orientation.

D. Module 3: Morphometry and Parameter-Space Analysis

The most important morphometries and parameter-space analyses performed as a part of this method are as follows.

1) Topographic Cross-Profile: The ratio between the end of the rim and the radius is defined in a range between 100% and 200% as parameter por. For each crater, up to s samples are taken for each different radial angle, wherein the relationship between r, por, s, and the sample of radius sor (position) is defined with (1a), (1b), (2a), and (2b). The elevation of samples around the crater center at location (x, y) are defined with (3a), (3b), and (4), wherein h is the height of digital topography data dtd and rr is the radial resolution. According to (5), topographic cross-profile tcp is defined as an average elevation at a distance of j from the crater center. While it is possible that some pixels from digital topography data may be sampled more than once on smaller craters and some others skipped on larger craters, this is not a problem due to a large sampling resolution. The result of this method is a 2-D representation of a 3-D crater shape

$$s = \min(r \cdot por/100, 128) \tag{1a}$$

$$sor = \max(9, r-1) \tag{1b}$$

$$s = (sor + 1) \cdot por/100 \tag{2a}$$

$$sor = s \cdot 100/por - 1 \tag{2b}$$

$$\lambda = 1/\cos(latitude) = 1/\sin(\pi \cdot y/(h-1)) \tag{3a}$$

$$\alpha_i = 2\pi \cdot i/rr \tag{3b}$$

$$el(\alpha_i, j) = dtd\left(x + \frac{r \cdot j}{sor} \cdot \cos(\alpha_i) \cdot \lambda, y + \frac{r \cdot j}{sor} \cdot \sin(\alpha_i)\right) \tag{4}$$

$$tcp(j) = \frac{1}{rr} \cdot \sum_{i=0}^{rr-1} el(\alpha_i, j). \tag{5}$$

2) Depth/Diameter Ratio: Once a minimum is found within the distance range between the crater's center and its radius, its depth is measured as a difference between the elevation at this minimum and the elevation at the crater's rim, according to (6). Having this value, d/D [15] can be computed as well

$$d = \max_{j=0}^{sor-1} \left(tcp(sor) - tcp(j)\right). \tag{6}$$

3) Circularity Analysis of Values in the Topography Data: To compute the circularity of a crater [51], the standard deviation of differences between elevation el and topography cross-profile tcp is computed according to (7). Once the sum of such values is computed for each distance from the crater's center according to (8a), the ratio between this area a_1 and area a_2 defined with (8b) is computed. Using circularity-probability parameter cpp_1 and (9a), the probability associated to circularity p_c can be computed as

$$delta(j) = \sqrt{\frac{1}{rr} \cdot \sum_{i=0}^{rr-1} \left(el(\alpha_i, j) - tcp(j)\right)^2} \tag{7}$$

$$a_1 = \sum_{j=0}^{sor} delta(j) \tag{8a}$$

$$a_2 = \sum_{j=0}^{sor} \left(tcp(sor) - tcp(j)\right) \tag{8b}$$

$$p_c = 10^{-\frac{cpp_1 \cdot a_1}{a_2}} \tag{9a}$$

$$p_{vc} = 10^{-\frac{vcpp_1 \cdot a_1'}{a_2'}}. \tag{9b}$$

4) Crater Rim: Similarly to a_1 and a_2, which represent roughness and the surface in tcp in the range between the center of a crater and its radius, appropriate values a_3 and a_4 are computed for the crater rim in the range between the radius and the end of a rim. Using these two values and rim-probability parameters rpp_1, rpp_2, rpp_3, and rpp_4, the probability associated to a crater rim p_{cr} can be computed according to

$$p_{\mathrm{cr}} = \left(1 - rpp_1 \cdot 10^{-\frac{rpp_2 \cdot a_3}{a_2}}\right) \cdot \left(1 - rpp_3 \cdot 10^{-\frac{rpp_4 \cdot a_3}{a_4}}\right). \tag{10}$$

5) Crater Central Peak: Similarly to a_3 and a_4, appropriate values a_5 and a_6 are computed for the central peak of a crater in the range between the center of a crater and the location of minimum defined with (6). Using these two values and central-peak-probability parameters $cppp_1$, $cppp_2$, $cppp_3$, and $cppp_4$, the probability associated to a crater central peak p_{cp} can be computed according to

$$p_{\mathrm{cp}} = \left(1 - cppp_1 \cdot 10^{-\frac{cppp_2 \cdot a_5}{a_2}}\right) \cdot \left(1 - cppp_3 \cdot 10^{-\frac{cppp_4 \cdot a_5}{a_6}}\right). \tag{11}$$

6) Radial Range Where a Crater Is Preserved: This method is invoked before the computation of the circularity and uses circularity computations in order to find the radial range where a crater is preserved. Once a_1 and a_2 are computed for this part, the rest of the measurements are performed for the complete radial range. This method uses the calibration in the form of function, which increases with the increase of radial range

where a crater is preserved. This is necessary in order to avoid computations for too small radial ranges.

7) Circularity Analysis of Votes in the Parameter Space: This method evaluates the parameter space in the same way as the circularity consistency evaluates the 3-D crater shape, as shown in (9b). The experiments show that the circularity of votes in the parameter space is higher at the craters' centers than in the centers of false detections. This is used in order to improve the overall performance.

E. Module 4: Probability Modification According to Radius

This method multiplies the probability that the detected feature is a crater (the product of all previously computed probabilities) by the calibration factor. The factor depends only on the detected radius and increases with the increase of the radius. This partially compensates for differences in morphology between large and small craters and ensures that the obtained crater diameter probability distribution is similar to the expected one for medium and large Martian craters.

F. Module 5: Slip Tuning of Crater Candidates

This method works as follows.

1) $delta$ is defined as two pixels.
2) For each crater candidate, 18 new crater candidates are defined, with $delta \cdot dr$ pixels smaller radius $(dr = -1)$, $delta \cdot dr$ pixels larger radius $(dr = 1)$, and coordinates of the center moved for $delta \cdot dx$ and $delta \cdot dy$ pixels east $(dx = 1)$, west $(dx = -1)$, north $(dy = 1)$, and south $(dy = -1)$.
3) For these 18 new crater candidates, the probability is reevaluated using all previous methods except the circularity analysis of votes in the parameter space which is not available at this stage.
4) The automated detection of smaller circular features inside a larger one (insider) and the automated depth/diameter measurement are performed.
5) If a crater candidate is labeled as an insider and some of the new crater candidates have larger computed probabilities, the new crater candidate is the one with the largest computed probability; otherwise, if a crater candidate is not labeled as an insider, it can be replaced with a new crater candidate if, in this case, the depth–diameter ratio is larger and the coordinates are the same or if the depth–diameter ratio is not smaller and the computed probability is larger.
6) Steps 2)–5) are repeated as long as "slipping" of the crater over the topography is possible.
7) The whole process is repeated with $delta$ decreased to one pixel.

For $delta$, we decided to use two as a startup value, since, in this case, results were better than for the other values (1, 3, etc.). We also experimented with a number of possible new crater candidates for each step, and we obtained the best results for the following 18 combinations: $\{dr, dx, dy\} \in \{\{+1, 0, 0\}, \{-1, 0, 0\}, \{0, +1, 0\}, \{0, -1, 0\}, \{0, 0, +1\}, \{0, 0, -1\}, \{0, +1, +1\}, \{0, -1, -1\}, \{0, +1, -1\}, \{0, -1, +1\}, \{+1, +1, 0\}, \{+1, -1, 0\}, \{+1, 0, +1\}, \{+1, 0, -1\}, \{+1, +1, +1\}, \{+1, -1, -1\}, \{+1, +1, -1\}, \{+1, -1, +1\}\}$.

G. Classification of Parameters and Their Interaction

The only parameters that are supposed to be changed by the user are the following: 1) r_1; 2) r_2; 3) *catalog-calibration values* (which can all be equal to 1); and 4) parameters specific for edge detectors (which can be used, as given in this paper). Other parameters need not be changed by the user, unless the user adds her/his own modules for additional morphometric measurements or works on improvements of ours. Other parameters are robust and only insignificantly interact with each other. The search for optimal parameter values is as follows: 1) We fixed all the values and searched for the optimum of the only selected parameter; 2) we did so for all the parameters; and 3) the complete process is repeated until no additional improvements are possible. All the values are found as optimal for CDA based on the gradient Canny (very similar results are obtained for CDA based on compass Canny) using the framework for evaluation of CDAs [6] including the GT-17582 catalog and 1/64° MOLA data.

III. Results

This section is organized as follows. In Section III-A, the results of the search for optimal parameter values are presented. In the framework for the evaluation of CDAs [6], it is described how the Free-response Receiver Operating Characteristics (F-ROC) can be used for the evaluation of CDAs. Therefore, the F-ROC-based evaluation of CDA performance presented in this paper is given in Section III-B. The quality of F-ROC-based evaluation depends significantly on the quality of the used GT catalog. Therefore, the reasoning for using GT-17582 and GT-57633 catalogs for evaluation is given in Section III-C. Section III-D describes the use of the presented CDA to perform the following: 1) search for still uncataloged craters and 2) extend the GT-57633 catalog significantly. In addition, the most important characteristics of the new GT-115225 catalog are presented. The largest and the smallest new craters from the GT-115225 catalog are of special concern because of the following reasons: 1) The largest craters come from the diameter range where the previous GT-57633 catalog is mostly complete, and 2) the smallest craters are in the diameter range where detection from MOLA data is problematic because of the grid size. The issues related to the largest and the smallest new craters are taken into account in Sections III-E and F. In Section III-G, a discussion of the criteria for the inclusion of new craters into the GT-115225 catalog is presented.

A. Optimal Values for Parameters

The optimal values for fixed parameters (not to be changed by the user) are as follows: $por = 148$, $cpp_1 = 0.74$, $vcpp_1 = 0.66$, $rpp_1 = 0.64$, $rpp_2 = 3.2$, $rpp_3 = 0.62$, $rpp_4 = 1.0$, $cppp_1 = 0.17$, $cppp_2 = 5.5$, $cppp_3 = 0.05$, $cppp_4 = 1.0$, and $radialcalibration = \{0.00, 0.10, 0.20, 0.30, 0.40, 0.50, 0.56, 0.74, 0.82, 0.85, 1.00\}$.

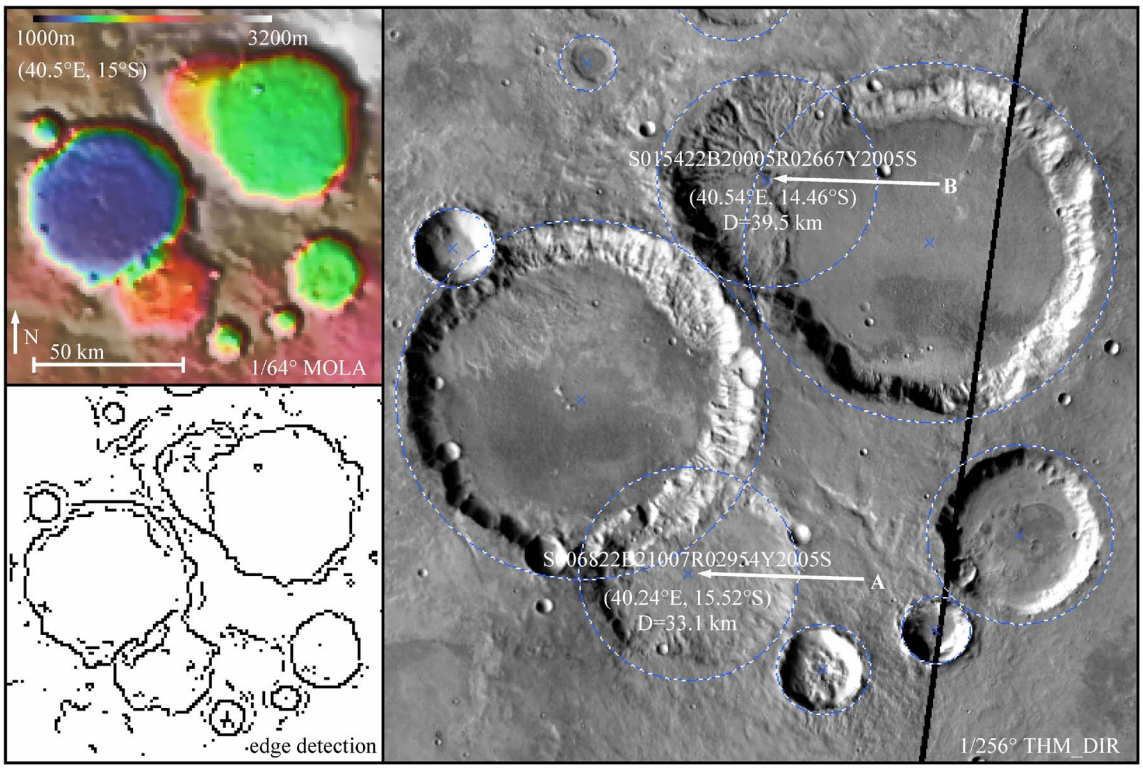

Fig. 2. (Top left) Digital topography data, (bottom left) the results of edge detection for Canny ($mask = 3 \times 3, \sigma = 0.25, r_1 = 5, r_2 = 28, grad_1 = grad_2 = 30$) operator, and (right) CDA's results for $p > 0.25$. Eroded crater A and heavily eroded crater B were detected, without false detections in this region and for these settings.

The ranges used for the other parameters are the following, wherein each corresponds to exactly one diameter range from Fig. 6 and their values have to be in ascending order: $2 \leq r_1 \leq 5$, $10 \leq r_2 \leq 28$, and $0 \leq catalog\text{-}calibrationvalues \leq 1$. The CDA based on Canny shows optimal performance for the following parameters: $kernel = 3$ (the size of the used mask), $\sigma = 0.25$ (defines the Gauss function), and $grad_1 = grad_2 = 30$ (gradients in ‰). The detected edges and craters are shown in Fig. 2. The optimal values for $catalogcalibration = \{0.10, 0.10, 0.10, 0.10, 0.10, 0.10, 0.48, 0.71, 0.81, 0.84, 0.95, 0.96, 0.96, 1.00, 1.00\}$. The optimal values for r_1 and r_2 were 5 and 10 before the modifications and are 5 and 28 for CDAs after the modifications given in this paper.

B. Evaluation of Performance Using F-ROC

The analysis using F-ROC and Area-Under F-ROC (AUROC) is shown in Fig. 3. For the evaluation of the results, the framework for the evaluation of CDAs was used, including 1/64° MOLA data and the GT-17582 catalog [6]. A detailed description of F-ROC, as well as an explanation of why AUROC can be used as a measure of CDA performance, is given in [6, Sec. 2.5, pp. 13–14]. The F-ROC-based evaluation can be outlined as follows: 1) Each CDA can be started using different parameters and different input data wherein, for each case, the result can be a different crater catalog; 2) for each such catalog and for a defined GT catalog, there is only one F-ROC curve (in order to satisfy this, before performing F-ROC, craters are automatically sorted in such a way that their order is always uniquely defined); 3) the F-ROC curve

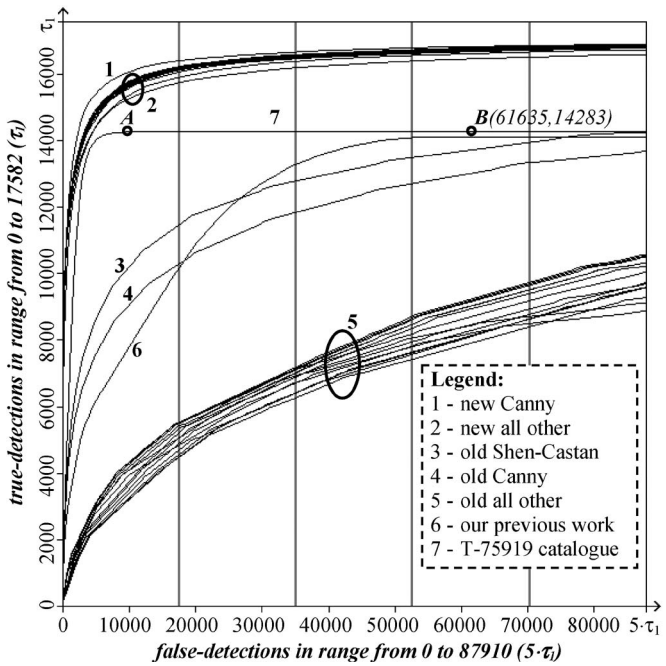

Fig. 3. F-ROC evaluations for different CDAs using GT-17582. CDAs after the modifications from this paper (1 and 2) are significantly better than the initial CDAs based on Shen–Castan (3) and Canny (4) approximately to the extent that they are better than the initial implementations of all other CDAs (5). The results for [6] (6) and [14] (7) were added for comparison purposes.

represents the number of correct versus false crater detections; and 4) there is a unique way to measure AUROC values from the curve. AUROC values are defined as the ratio between

the area under F-ROC and the area up to the horizontal line defined by the number of craters from a GT catalog [6]. The $AUROC_{\{1,2,5\}\tau} = \{X\%, Y\%, Z\%\}$ means that values X, Y, and Z correspond to AUROC's τ, 2τ and 5τ false detections, respectively.

Examples of points on the curve are A and B, as shown in curve 7 in Fig. 3. Point B corresponds to the 14 283 craters from the T-75919 catalog [14] found in the GT-17582 catalog [6] and to the remaining 61 635 craters that were not found (the sum is for one crater smaller than 75 919 because one crater was detected as duplicate and deleted before the F-ROC analysis). The craters between points A and B are too small for the evaluation using the GT-17582 catalog.

It should be noticed that the craters from catalog T-75919 [14] are given without probabilities of detection. In principle, this defines only a single point B in Fig. 3, according to [6]. It is possible to draw a line between (0, 0) and this point and a horizontal line between this point and the rightmost edge of the graph. However, this would considerably underestimate the performance of this CDA in comparison with others that provide the probability of detection for each crater. Our solution was the sort order: probability, radius, longitude, and latitude (descending for all). Therefore, larger craters are evaluated first, which gives better results for the GT-17582 catalog and more comparable results for other CDAs.

The results for the CDA from the previous work [6] are as follows: $gt = 14\,134/17\,582$ (detected craters) and $AUROC_{\{1,2,5\}\tau 1} = \{40.314\%, 54.359\%, 69.472\%\}$. The results for the CDA from this paper (gradient version of Canny–RH) are as follows: $gt = 17\,017/17\,582$ and $AUROC_{\{1,2,5\}\tau 1} = \{87.075\%, 90.567\%, 93.543\%\}$. When the same CDA is used with 1/128° MOLA data, the results are the following: $gt = 17\,108/17\,582$ and $AUROC_{1,2,5\tau 1} = \{86.555\%, 90.444\%, 93.719\%\}$. The compass version of Canny–RH shows very similar performance. For the CDA which resulted in the T-75919 catalog [14] and used the same 1/128° MOLA data as input and was evaluated using the same GT-17582 catalog, the results are as follows: $gt = 14\,283/17\,582$ and $AUROC_{\{1,2,5\}\tau 1} = \{74.366\%, 77.746\%, 79.775\%\}$. These results are also very good; therefore, it is not a surprise that the results of the evaluation using the GT-57633 catalog show that this CDA is better in some segments than the CDA (1) from Fig. 3, as shown in Fig. 4. However, when 1/128° MOLA data are used as a source, r_1 is changed from 5 to 4, and $catalogcalibration = \{0.41, 0.41, 0.41, 0.41, 0.52, 0.61, 0.74, 0.92, 0.99, 1.00, 1.00, 1.00, 1.00, 1.00, 1.00\}$ is used, the results for the CDA presented in this paper are better again in all segments, as shown in Fig. 4.

For most planetary science applications, only the range of parameters where the value on the x-axis of the F-ROC curves is significantly smaller than the value on the y-axis makes sense, which represents high sensitivity and specificity. Therefore, the values of AUROC for 2τ and 5τ are not helpful and not shown in Fig. 4. This is also not the case for Fig. 3, wherein the older GT-17582 catalog was used, because in this case, interesting portions of the curves would not be shown. Another point is the case when the application of CDA is to search for still uncataloged craters, which is the subject of this paper.

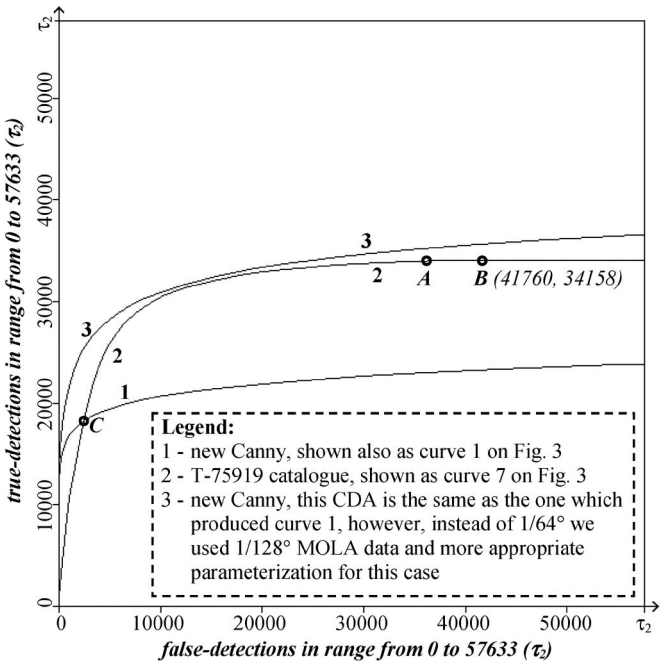

Fig. 4. F-ROC evaluations for different CDAs using GT-57633. CDA (1) outperforms CDA (2) [14], but only before point C. The reason is that CDA (1) mostly searches for large craters, while the catalog from CDA (2) contains lots of small craters which are in GT-57633 and not in the GT-17582 catalog. CDA (3) provides better results than the other two.

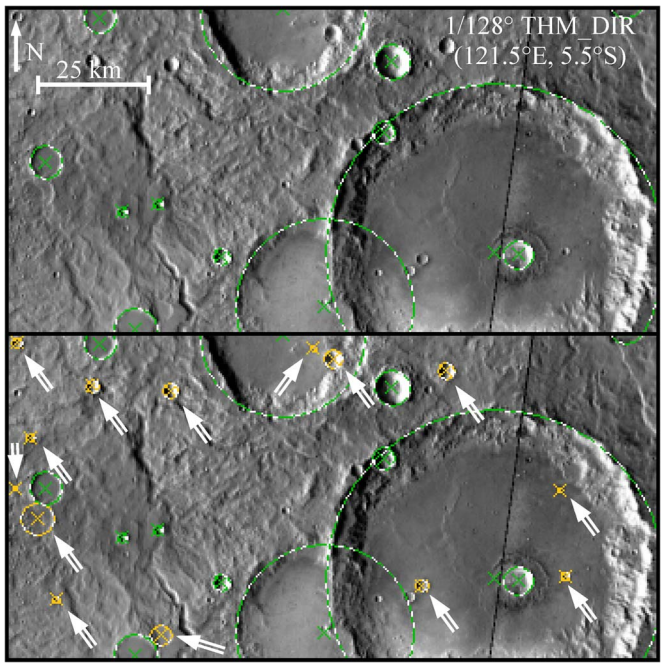

Fig. 5. Part of (top) the initial GT-57633 catalog of Martian impact craters and (bottom) the resulting GT-115225 catalog. It can be noticed that numerous new craters were detected using a Canny-based CDA from this paper and confirmed as correct detections. They contributed to the significant extension of the previous GT-57633 catalog, with 57 592 new craters.

C. Reasoning for Used Ground-Truth

Both the CDA which was used to produce catalog T-75919 [14] and the CDA presented in this paper detect small craters much less precisely (particularly, D is overestimated) than large ones due to the limitations inherent to DEM. Consequently,

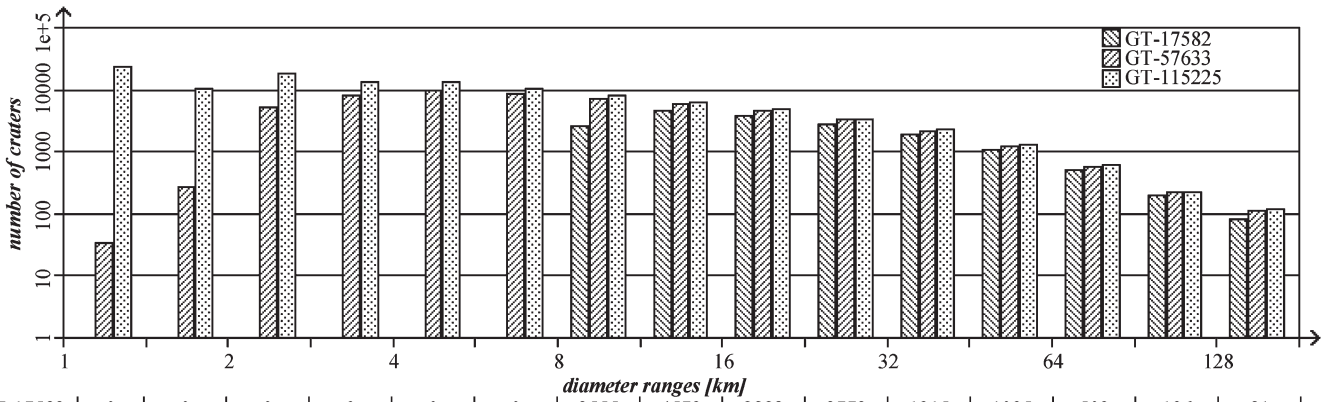

GT-17582	0	0	0	0	0	0	2555	4573	3892	2772	1915	1095	503	196	81
GT-57633	33	277	5226	8085	9780	8822	7293	5888	4550	3311	2206	1246	579	222	115
GT-115225	22811	10561	17823	13264	13508	10143	8050	6316	4807	3450	2270	1282	597	227	116
new 57592	22778	10284	12603	5173	3727	1323	756	428	258	137	63	38	18	5	1
new in %	99.86	97.38	70.71	39.00	27.59	13.04	9.39	6.78	5.37	3.97	2.78	2.96	3.02	2.20	0.86

Fig. 6. Distribution of craters from catalogs GT-17582, GT-57633, and GT-115225. The chart represents log10 of the number of craters for the corresponding diameter range. The values shown in the chart are given in the first three rows. In the fourth row, the distribution of craters found with the CDA from this paper is given. They are not always the difference between the values from the third and second rows, because during the registration of the newly found 57 592 craters, we also corrected the location and the diameter of some craters from the GT-57633 catalog; therefore, some craters changed correspondingly with the range. The fifth row is the percentage of the newly found craters in the GT-115225 catalog.

the algorithm for the automated matching of craters cannot successfully match such craters with the craters from the GT catalog and therefore labels them as false detections, as shown in Fig. 4. The main reason why we are still using the GT-17582 catalog is that these problems are not inherent to large craters; thus, it is easier to estimate how many craters are not detectable by a particular CDA. On the other hand, the GT-57633 catalog is much more complete than the GT-17582 catalog and, in fact, contains all the craters from the GT-17582 catalog plus numerous others. Therefore, using the GT-57633 catalog (to test the performance of CDAs) results in a larger number of true detections; hence, this approach is better for estimating how many craters are detected by a CDA. Additional reasons for the use of GT-57633 are as follows: 1) By using an automated approach, it was possible to find more craters in this catalog; therefore, there were less to check manually, and 2) without this catalog, it would not be possible to know how many craters were found by major human labelers until now and how many craters were found by our CDA.

It is difficult to have any ground truth (GT), because human counters are always missing some craters; hence, no manually constructed catalog—much less a global catalog—is totally complete to constitute a real GT. There is always the option to select a region, to create (or manually correct) a GT for this region, and then, to use this as the basis for assessment of the performance of a CDA. However, one of the consequences resulting from difficulties in having any GT is the question of objectivity of such evaluation. Another problem is the selection of representative regions. We noticed that both the CDA which resulted in catalog T-75919 [14] and the CDA from this paper are very good for some regions and have problems with others (mostly complex terrains). Therefore, the usage of a global GT catalog, which contains only the craters either found or confirmed by nonauthors of CDAs, brings numerous important advantages.

D. Construction of the New GT-115225 Catalog

For the CDA from this paper, achieved detection rates (for $gt = 17\,108/17\,582$ only $\sim$2.7% of craters are undetected) occur when all 193 402 craters with the highest probability are taken into account. In such a case, the number of false detections is larger than the number of correct detections, due to the CDA's greater sensitivity. However, this was necessary in order to find as many uncataloged craters as possible. One of the target purposes is that crater statistics can be used, in a statistically significant way, for better understanding of global geological processes [32], [33]. Therefore, the strategy for the detection of craters and the construction of the new catalog was to perform the detection for the entire planet and not for some preferential regions related to some particular geological period. As the first step, we changed the 1/64° MOLA data that we used for tuning of parameters and evaluation with 1/128° MOLA data, and we set all catalog-calibration values to 1. First, 157 840 (193 402 minus all found in GT-57633) craters were manually analyzed, and the GT-57633 catalog was extended by 5985 new craters. In the following steps, we decreased r_1 to four, three, and two pixels, additionally manually analyzed 77 629 (193 402 minus all from GT-57633 and minus all when r_1 is equal to 5), 80 460 (193 402 minus all from GT-57633 and minus all when r_1 is equal to 5 and 4), and 98 702 (193 402 minus all from GT-57633 and minus all when r_1 is equal to 5, 4, and 3) craters, and extended the catalog with 5047, 9463, and 37 097 new craters. Altogether, 414 631 craters were analyzed, and 57 592 were confirmed as correct detections. As for all the previous craters from the GT-57633 catalog, registration was performed for all visual images, and the coordinates and the radius were manually adjusted where necessary. A sample from the resulting catalog is shown in Fig. 5, and the distribution of craters is shown in Fig. 6.

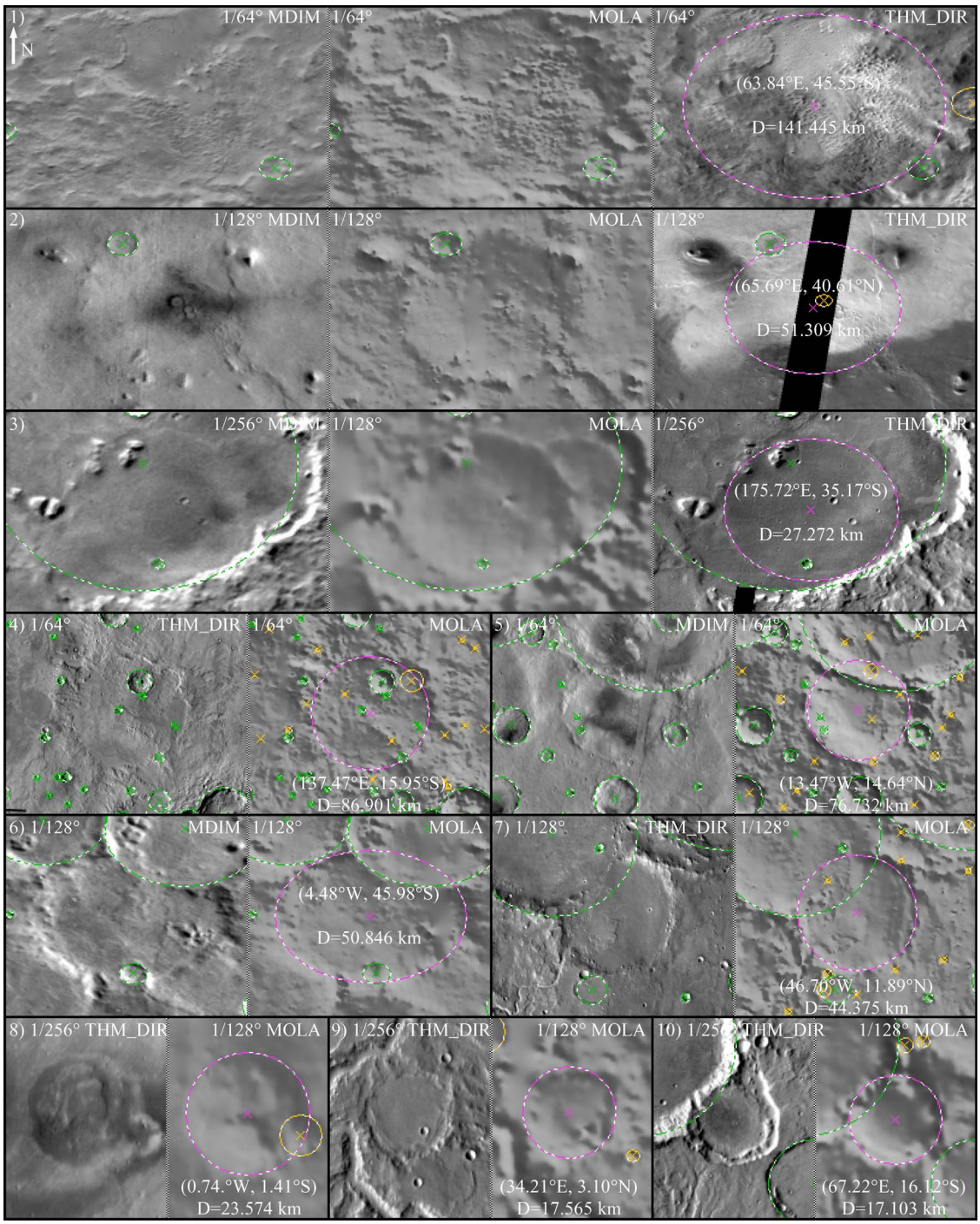

Fig. 7. Three newly found large craters, which are not visible in an image but are still present in topography, are shown as the examples for (1) $D > 64$ km S061933L042573Y2009S, (2) 64 km $> D >$ 32 km S060937L038709Y2009S, and (3) 32 km $> D >$ 16 km S059179L003332Y2009S. Seven newly found large craters that were missed by human labelers are shown as the examples for the same diameter ranges, S061610L029473Y2009S (4), S061135L030357Y2009S (5), S059253L002378Y2009S (6), S060194L011558Y2009S (7), S060326L012804Y2009S (8), S058846L004130Y2009S (9), and S058505L001644Y2009S (10).

E. Largest New Craters From GT-115225 Catalog

In the GT-115225 catalog, there are 42 218 craters with $D > 5$ km, and in the GT-57633 catalog, there are 38 085 such craters. This means that we detected 4133 previously uncataloged craters with $D > 5$ km. This number is slightly smaller than the 5985 craters registered for the case when r_1 was 5, because during the registration in the GT catalog, the detected diameter was usually corrected to some smaller value. However, these 4133 craters are still ∼10% of the 42 218 craters, which can be interpreted as showing that the manual mappers have missed ∼10% of large craters on Mars. However, these numbers could be misleading. With the first extension of the GT-17582 catalog, we found 1129 craters [7], for which, in catalog B, $D < 10$ km, and in catalog R, $D > 10$ km. This effect was actually the only reason why these craters were not registered in the GT-17582 catalog in the first place.

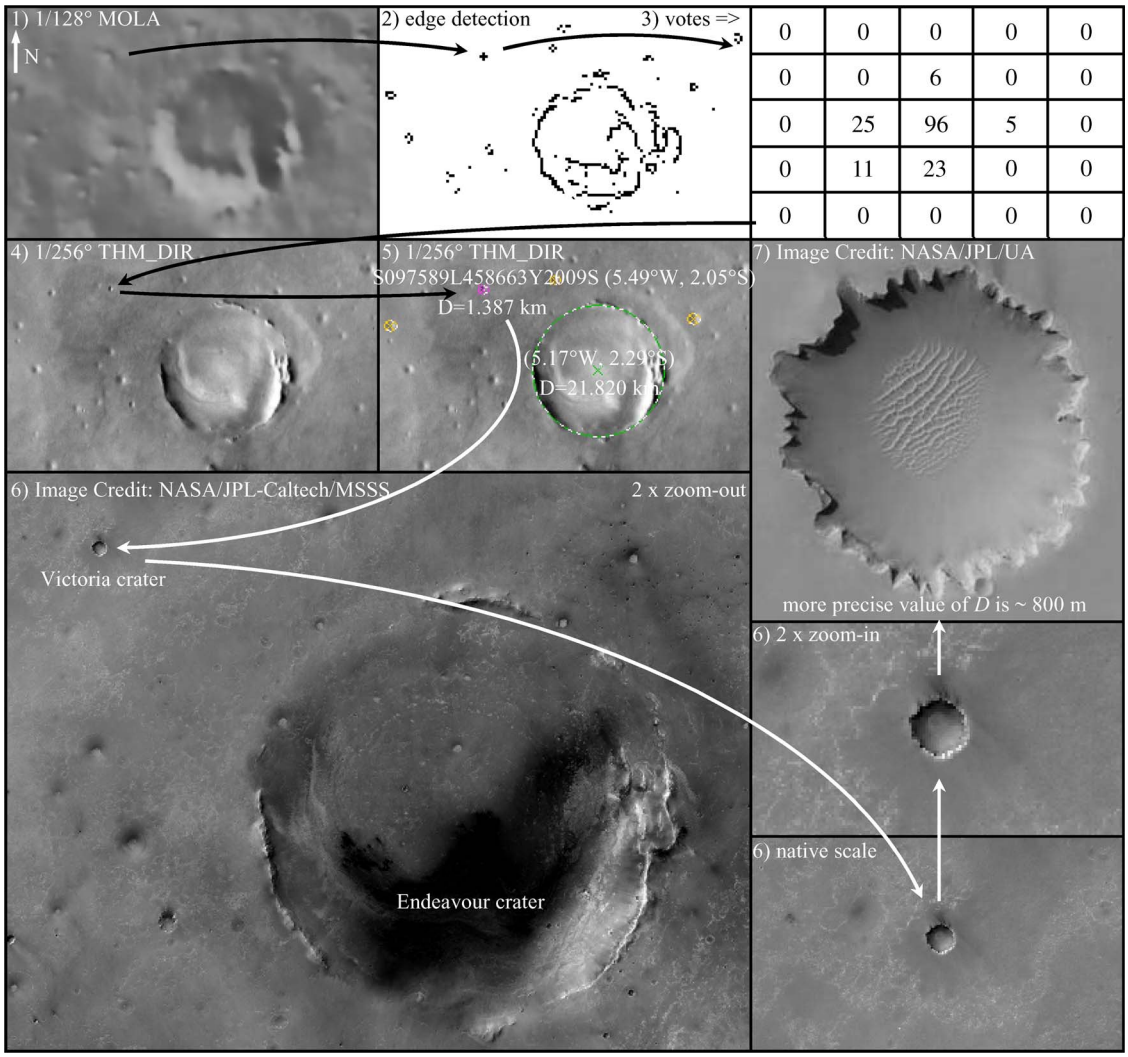

Fig. 8. Illustration of the detection of small craters. For (1) 1/128° MOLA data, (2) the results of fuzzy edge detection are shown, wherein the small depression resulted with a small cross. The results of fuzzy RH transform (votes) are additionally shown, wherein, at the location (22 336, 11 782), (3) there is a maximum of 96 votes. During the manual review, (4) 1/256° THM_DIR and MDIM were checked, and (5) upon the decision that the detection indeed is a crater, it was registered into the GT. We checked some higher resolution images (6) and (7) and found out that the detection is actually the Victoria crater. Image (6) (downloaded from http://www1.nasa.gov/mission_pages/mer/images/pia11837.html) is the context image of the Endeavour and Victoria craters: The largest crater in this mosaic of images taken by the Context Camera on NASA's Mars Reconnaissance Orbiter is the Endeavour crater; the much smaller crater at the top left corner is the Victoria crater. Image (7) (downloaded from http://www.nasa.gov/mission_pages/MRO/multimedia/pia08813.html) is a portion of an image taken by the High Resolution Imaging Science Experiment camera onboard the Mars Reconnaissance Orbiter spacecraft. Please note that, for illustration purposes, the black arrows represent the steps done for all craters and the white arrows show what we did only for this (Victoria) crater.

Additionally, this catalog contains only those craters that are in both catalogs B and R. For $D > 10$ km, in GT-17582, there are 16 933, in GT-57633, there are 20 591, and in GT-115225, there are 21 786 such craters. This means that the ∼5.49% extension from this paper with 1195 ($21\,786 - 20\,591$) such craters is partially explained by the previous ∼17.77% extension with 3658 ($20\,591 - 16\,933$) such craters, wherein it is known that each of them missed at least catalog B or R. Additional 2938 $(4133 - 1195)$ craters come from range $10 \text{ km} > D > 5$ km, not covered by catalog R and covered only by one global catalog, namely, B; hence, the fact that they were missed by only one labeler was not a surprise. However, most of the newly found large craters are indeed much degraded, usually not visible in an image, but still present in topography. Three of such cases are shown in the first three parts of Fig. 7. However, there are also some craters that are simply missed by human labelers. Seven of such cases are shown in the last three parts of Fig. 7.

F. Smallest New Craters From GT-115225 Catalog

The extension of the GT-57633 catalog with 4133 craters with $D > 5$ km means that it was extended with 53 459 $(57\,592 - 4133)$ craters smaller than 5 km. For very small craters, the calculation of diameter and depth is very questionable, as well as the calculation of all other properties used for the detection. However, some very small craters that look degraded because of the resolution limitation can still be detected, owing to the robustness and versatility of the approach. This does not mean that we recommend our CDA to be used with r_1 as small as two pixels. However, we wanted to push our CDA to the limits to see what results can be obtained. At the end, we decided to check at least one such detection of a very small crater with some known crater using higher resolution images than 1/256°. As shown in Fig. 8, even the Victoria crater (famous for the nearby rower) was successfully detected. The facts are as follows: 1) This single case is certainly statistically

insignificant; 2) this crater was detected with an overestimated diameter of 1.387 km instead of ∼800 m; and 3) the location contains a similar relative error ($\pm 1 \sim 2$ pixels). However, this was still a nice surprise because ∼800 m in diameter is less than two pixels in diameter on 1/128° MOLA data, and the crater was still detected.

G. Criteria for Inclusion Into GT-115225 Catalog

During the inclusion of the craters found by the CDA in the GT catalog, in some cases (for large very degraded craters and for very small craters), it was a real challenge to verify CDA decisions (differentiate actual craters versus false detections only similar to craters). Some labelers add craters to catalogs only if they are absolutely confident that they are craters indeed, while others, even if chances are much higher that the feature is not a crater, still decide to add it. Our reasoning was the same as during the work on the GT-57633 catalog. If the judgment is that it is more likely that the detected object is an impact crater, the crater is included into the catalog; otherwise, it is deleted.

IV. Conclusion

The main findings are as follows: 1) The new CDA presented in this paper has shown significantly better crater detection results than other published methods; 2) the developed methods can be used for automated morphometry measurements [52]; and 3) using the resulting CDA, the initial GT-57633 catalog is significantly extended by 57 592 previously uncataloged craters. The resulting new GT-115225 catalog contains significantly more craters than any previous catalog. From this point of view, it is currently one of the most complete catalogs of medium to large Martian impact craters.

The successful detection of fresh well-formed craters is not hard to achieve. However, the detection of eroded craters as well as the craters which are partially erased is challenging because, with the increase of sensitivity, the number of false detections increases as well. Owing to the performance achieved by the CDAs described in this paper, the increase of false detections is significantly smaller than for the initial CDAs, even in modes where CDAs are highly sensitive. As a result and despite the large number of manually checked crater candidates, the number of newly found previously uncataloged craters is significant as well.

The goal of the future work is to integrate the new GT catalog with the following: 1) the T-75919 catalog [14] and 2) the manually assembled catalog [42] with over 280 000 craters [53] (once it is available). In order to provide more precise evaluation, we also plan to extend the framework for evaluation of CDAs [6] with 1/128° MOLA data, 1/256° visual images, and a more complete catalog for GT [7] and develop a more advanced algorithm for the evaluation of CDAs and crater catalogs.

Acknowledgment

The authors would like to thank the referees for their helpful and valuable comments and suggestions for the improvement of the quality and clarity of the manuscript; T. F. Stepinski for providing the catalog with 75 919 craters; H. Novosel and H. Knežević for contributing to the work on edge detectors; and D. Gržanić, M. Karas, D. Katušić, S. Katušić, M. Kovač, J. Lucić, D. Mehić, D. Prelošćan, V. Primorac, N. Rizvanović, B. Spasić, D. Stilinović, Lj. Šare, and D. Zorić for providing computers for the cluster which was used for the computation of the optimal parameters for 17 different CDAs.

References

[1] F. Schmidt, S. Douté, and B. Schmitt, "WAVANGLET: An efficient supervised classifier for hyperspectral images," *IEEE Trans. Geosci. Remote Sens.*, vol. 45, no. 5, pp. 1374–1385, May 2007.

[2] D. Tuia, F. Ratle, F. Pacifici, M. F. Kanevski, and W. J. Emery, "Active learning methods for remote sensing image classification," *IEEE Trans. Geosci. Remote Sens.*, vol. 47, no. 7, pp. 2218–2232, Jul. 2009.

[3] S. Ghosh, T. F. Stepinski, and R. Vilalta, "Automatic annotation of planetary surfaces with geomorphic labels," *IEEE Trans. Geosci. Remote Sens.*, vol. 48, no. 1, pp. 175–185, Jan. 2010.

[4] T. F. Stepinski and C. Bagaria, "Segmentation-based unsupervised terrain classification for generation of physiographic maps," *IEEE Geosci. Remote Sens. Lett.*, vol. 6, no. 4, pp. 733–737, Oct. 2009.

[5] A. M. Fernandes, "Study on the automatic recognition of oceanic eddies in satellite images by ellipse center detection—The Iberian coast case," *IEEE Trans. Geosci. Remote Sens.*, vol. 47, no. 8, pp. 2478–2491, Aug. 2009.

[6] G. Salamunićcar and S. Lončarić, "Open framework for objective evaluation of crater detection algorithms with first test-field subsystem based on MOLA data," *Adv. Space Res.*, vol. 42, no. 1, pp. 6–19, Jul. 2008.

[7] G. Salamunićcar and S. Lončarić, "GT-57633 catalogue of Martian impact craters developed for evaluation of crater detection algorithms," *Planet. Space Sci.*, vol. 56, no. 15, pp. 1992–2008, Dec. 2008.

[8] G. R. J. Cooper, "Feature detection using sun shading," *Comput. Geosci.*, vol. 29, no. 8, pp. 941–948, Oct. 2003.

[9] J.-R. Kim, J. L. Simpson, J.-P. Muller, and S.-Y. Lin, "3D crater data base construction using automated and manual components for crater morphology," *Geophys. Res. Abstr.*, vol. 10, Apr. 2008, no. EGU2008-A-11490.

[10] J. I. Simpson, J. R. Kim, and J.-P. Muller, "3D crater database production on Mars by automated crater detection and data fusion," in *Proc. 21st ISPRS Congr.*, Beijing, China, Jul. 2008, pp. 1049–1054.

[11] S. O. Krøgli, H. Dypvik, and B. Etzelmüller, "Automatic detection of circular depressions in digital elevation data in the search for potential Norwegian impact structures," *Norwegian J. Geol.*, vol. 87, no. 1/2, pp. 157–166, 2007.

[12] R. Martins, P. Pina, J. S. Marques, and M. Silveira, "A boosting algorithm for crater detection," presented at the Visualization, Imaging, Image Processing Conf., Palma de Mallorca, Spain, Sep. 2008.

[13] R. Martins, P. Pina, J. S. Marques, and M. Silveira, "Crater detection by a boosting approach," *IEEE Geosci. Remote Sens. Lett.*, vol. 6, no. 1, pp. 127–131, Jan. 2009.

[14] T. F. Stepinski and E. R. Urbach, "Completion of the first automatic survey of craters on Mars," presented at the 11th Mars Crater Consortium Meeting, Flagstaff, AZ, Sep. 2008.

[15] T. F. Stepinski and E. R. Urbach, "The first automatic survey of impact craters on Mars: Global maps of depth/diameter ratio," presented at the 40th Lunar Planetary Science Conf., The Woodlands, TX, Mar. 2009, Abs. 1117.

[16] E. R. Urbach and T. F. Stepinski, "Automatic detection of sub-km craters in high resolution planetary images," *Planet. Space Sci.*, vol. 57, no. 7, pp. 880–887, Jun. 2009.

[17] T. F. Stepinski, M. P. Mendenhall, and B. D. Bue, "Machine cataloging of impact craters on Mars," *Icarus*, vol. 203, no. 1, pp. 77–87, Sep. 2009.

[18] G. Salamunićcar and S. Lončarić, "Circular-consistency and slip-tuning improvements of crater detection algorithms based on gradient edge detectors and Radon/Hough transform," presented at the 7th Int. Conf. Mars, Pasadena, CA, Jul. 2007, Abs. 3066.

[19] H. Knežević, G. Salamunićcar, and S. Lončarić, "Crater detection algorithms based on Prewitt, Abdou, Argyle, Macleod, Derivative-of-Gaussian and Canny gradient edge detectors," presented at the 39th Lunar Planetary Science Conf., League City, TX, Mar. 2008, Abs. 1378.

[20] G. Salamunićcar and S. Lončarić, "Gradient amplification and gradient orientation improvements of crater detection algorithms based on edge detectors and Radon/Hough transform," presented at the 39th Lunar Planetary Science Conf., League City, TX, Mar. 2008, Abs. 1375.

[21] G. Salamunićcar and S. Lončarić, "Morphometry, votes-analysis and calibration improvements of crater detection algorithms based on edge detectors and Radon/Hough transform," presented at the 40th Lunar Planetary Science Conf., The Woodlands, TX, Mar. 2009, Abs. 1084.

[22] A. Bijaoui and M. M. Froeschle, "A new algorithm to determine image edges—Application to lunar craters," *Astron. Astrophys.*, vol. 87, no. 1/2, pp. 250–251, Jul. 1980.
[23] J. R. Kim, J.-P. Muller, S. van Gasselt, J. G. Morley, and G. Neukum, "Automated crater detection, a new tool for Mars cartography and chronology," *Photogramm. Eng. Remote Sens.*, vol. 71, no. 10, pp. 1205–1217, Oct. 2005.
[24] Y. Sawabe, T. Matsunaga, and S. Rokugawa, "Automated detection and classification of lunar craters using multiple approaches," *Adv. Space Res.*, vol. 37, no. 1, pp. 21–27, 2006.
[25] A. Chicarro, G. Michael, P. G. Marchetti, M. Costantini, F. Di Stadio, and M. Di Martino, "Unravelling the Earth's geological history from space using impact craters," *ESA Bull.*, no. 114, pp. 68–75, May 2003.
[26] Y. Cheng, J. Goguen, A. Johnson, C. Leger, L. Matthies, M. S. Martin, and R. Willson, "The Mars exploration rovers descent image motion estimation system," *IEEE Intell. Syst.*, vol. 19, no. 3, pp. 13–21, May/Jun. 2004.
[27] A. Johnson, R. Willson, J. Goguen, J. Alexander, and D. Meller, "Field testing of the Mars exploration rovers descent image motion estimation system," in *Proc. IEEE Int. Conf. Robot. Autom.*, Barcelona, Spain, Apr. 2005, pp. 4463–4469.
[28] B. Leroy, G. Medioni, E. Johnson, and L. Matthies, "Crater detection for autonomous landing on asteroids," *Image Vis. Comput.*, vol. 19, no. 11, pp. 787–792, Sep. 2001.
[29] R. Li, F. Ma, F. Xu, L. H. Matthies, C. F. Olson, and R. E. Arvidson, "Localization of Mars rovers using descent and surface-based image data," *J. Geophys. Res.*, vol. 107, no. E11, pp. 1–8, Aug. 2002.
[30] M. Maimone, A. Johnson, Y. Cheng, R. Willson, and L. Matthies, "Autonomous navigation results from the Mars exploration rover (MER) mission," presented at the 9th Int. Symp. Experimental Robotics, Singapore, Jun. 2004.
[31] G. G. Michael, "Coordinate registration by automated crater recognition," *Planet. Space Sci.*, vol. 51, no. 9/10, pp. 563–568, Aug. 2003.
[32] G. Salamunićcar, "Applying the mathematical theory of stochastic processes to lunar and planetary science: The ancient oceans on Mars case," *Adv. Space Res.*, vol. 33, no. 12, pp. 2281–2287, Jun. 2004.
[33] G. Salamunićcar, "The first new application of the mathematical theory of stochastic processes to lunar and planetary science: Topography-profile diagrams of Mars," *Adv. Space Res.*, vol. 43, no. 2, pp. 308–316, Jan. 2009.
[34] G. Salamunićcar and D. Selar-Glavočić, "Image processing algorithms for visualization of quasi-circular-depressions: A step toward the automatic process of detection and classification of Martian buried impact craters," presented at the 6th Int. Conf. Mars, Pasadena, CA, Jul. 2003, Abs. 3202.
[35] G. Salamunićcar and S. Lončarić, "Estimation of false detections for evaluation of crater detection algorithms," presented at the 37th Lunar Planetary Sci. Conf., League City, TX, Mar. 2006, Abs. 1138.
[36] W. Frei and C.-C. Chen, "Fast boundary detection: A generalization and a new algorithm," *IEEE Trans. Comput.*, vol. C-26, no. 10, pp. 988–998, Oct. 1977.
[37] S. R. Deans, "Hough transform from the Radon transform," *IEEE Trans. Pattern Anal. Mach. Intell.*, vol. PAMI-3, no. 2, pp. 185–188, Mar. 1981.
[38] H. Novosel, G. Salamunićcar, and S. Lončarić, "Crater detection algorithms based on pixel-difference, separated-pixel-difference, Roberts, Prewitt, Sobel and Frei–Chen gradient edge detectors," presented at the 38th Lunar Planetary Science Conf., League City, TX, Mar. 2007, Abs. 1351.
[39] W. K. Pratt, *Digital Image Processing: PIKS Inside*, 3rd ed. New York: Wiley, 2001, pp. 443–508.
[40] J. F. Canny, "A computational approach to edge detection," *IEEE Trans. Pattern Anal. Mach. Intell.*, vol. PAMI-8, no. 6, pp. 679–698, Nov. 1986.
[41] J. Shen and S. Castan, "An optimal linear operator for step edge detection," *Comput. Vis. Graph. Image Process.: Graph. Models Image Process.*, vol. 54, no. 2, pp. 112–133, Mar. 1992.
[42] S. J. Robbins and B. M. Hynek, "Towards a new catalog of lobed Martian craters compared with a new global crater database, complete to 1.5 km," presented at the 40th Lunar Planetary Science Conf., The Woodlands, TX, Mar. 2009, Abs. 2460.
[43] L. Bandeira, J. Saraiva, and P. Pina, "Impact crater recognition on Mars based on a probability volume created by template matching," *IEEE Trans. Geosci. Remote Sens.*, vol. 45, no. 12, pp. 4008–4015, Dec. 2007.
[44] H. V. Frey, J. H. Roark, K. M. Shockey, E. L. Frey, and S. E. H. Sakimoto, "Ancient lowlands on Mars," *Geophys. Res. Lett.*, vol. 29, no. 10, pp. 22.1–22.4, May 2002.
[45] T. R. Watters, C. J. Leuschen, J. J. Plaut, G. Picardi, A. Safaeinili, S. M. Clifford, W. M. Farrell, A. B. Ivanov, R. J. Phillips, and E. R. Stofan, "MARSIS radar sounder evidence of buried basins in the northern lowlands of Mars," *Nature*, vol. 444, no. 7121, pp. 905–908, Dec. 2006.
[46] K. Tsutsui, S. Rokugawa, H. Nakagawa, S. Miyazaki, C.-T. Cheng, T. Shiraishi, and S.-D. Yang, "Detection and volume estimation of large-scale landslides based on elevation-change analysis using DEMs extracted from high-resolution satellite stereo imagery," *IEEE Trans. Geosci. Remote Sens.*, vol. 45, no. 6, pp. 1681–1696, Jun. 2007.
[47] B. D. Bue and T. F. Stepinski, "Machine detection of Martian impact craters from digital topography data," *IEEE Trans. Geosci. Remote Sens.*, vol. 45, no. 1, pp. 265–274, Jan. 2007.
[48] N. G. Barlow, C. W. Barnes, O. S. Barnouin-Jha, J. M. Boyce, C. R. Chapman, F. M. Costard, R. A. Craddock, J. B. Garvin, R. Greeley, T. M. Hare, R. O. Kuzmin, P. J. Mouginis-Mark, H. E. Newsom, S. E. H. Sakimoto, S. T. Stewart, and L. A. Soderblom, "Utilizing GIS in Martian impact crater studies," presented at the ISPRS WG IV/9 Extraterrestrial Mapping Workshop: Advances Planetary Mapping 2003, League City, TX, Mar. 2003.
[49] H. J. Melosh and B. A. Ivanov, "Impact crater collapse," *Annu. Rev. Earth Planet. Sci.*, vol. 27, pp. 385–415, 1999.
[50] C. Sanchez-Hernandez, D. S. Boyd, and G. M. Foody, "One-class classification for mapping a specific land-cover class: SVDD classification of Fenland," *IEEE Trans. Geosci. Remote Sens.*, vol. 45, no. 4, pp. 1061–1073, Apr. 2007.
[51] J. Earl, A. F. Chicarro, C. Koeberl, P. G. Marchetti, and M. Milnes, "Automatic recognition of crater-like structures in terrestrial and planetary images," presented at the 36th Lunar Planetary Science Conf., League City, TX, Mar. 2005, Abs. 1319.
[52] G. Salamunićcar and S. Lončarić, "Automated depth/diameter and topographic-cross-profile measurements based on GT-57633 catalogue of Martian impact craters and MOLA data," presented at the 40th Lunar Planetary Science Conf., The Woodlands, TX, Mar. 2009, Abs. 1085.
[53] S. J. Robbins and B. M. Hynek, "Progress towards a new global catalog of Martian craters and layered ejecta properties, complete to 1.5 km," presented at the 12th Mars Crater Consortium Meeting, Flagstaff, AZ, Sep. 2009.

Goran Salamunićcar (M'98) received the B.Sc. degree in electrical engineering and the M.Sc. degree in computer science from the Faculty of Electrical Engineering and Computing, University of Zagreb, Zagreb, Croatia, in 1996 and 2000, respectively, where he is currently working toward the Ph.D. degree, with a focus on crater detection algorithms that utilize digital topography data.

He has been a Software Developer for more than 11 years, first with PELSYS d.o.o. and currently with AVL-AST d.o.o., Zagreb. He has been teaching object-oriented software development at the Polytechnic of Zagreb, Croatia, since 2002. He has been volunteering as a Membership Officer of Mensa Croatia since 2003. He is the author (or coauthor) of four scientific publications in refereed international journals, one patent, and 34 scientific publications in conference proceedings.

Mr. Salamunićcar is a member of the Association for Computing Machinery, American Geophysical Union, American Association for the Advancement of Science, and Mensa Croatia. He is also an Associate of the Committee on Space Research and the Mars Exploration Program Analysis Group.

Sven Lončarić (M'90–SM'03) received the B.Sc. and M.Sc. degrees in electrical engineering from the University of Zagreb, Zagreb, Croatia, in 1985 and 1989, respectively, and the Ph.D. degree in electrical engineering from the University of Cincinnati, Cincinnati, OH, in 1994.

From 1990 to 1994, he was a Fulbright Fellow and a Research Assistant with the University of Cincinnati. He was an Assistant Professor with the New Jersey Institute of Technology, Newark, from 2001 to 2003. He has been a Full Professor with the University of Zagreb since 2006, where he was an Assistant Professor from 1996 to 2001 and an Associate Professor from 2001 to 2006. Currently, he is the Chair of the Department of Electronic Systems and Information Processing, Faculty of Electrical Engineering and Computing, University of Zagreb. He is a coauthor of more than 120 refereed journal and conference publications. He has been the Editor-in-Chief of the *Journal of Computing and Information Technology*.

Dr. Lončarić served as the IEEE Croatia Section Chair from 2005 to 2008 and was the Founder and the Chair of the IEEE Croatia Section Computational Intelligence Society Chapter.